Volume 4, Issue 6, June 2026 ISSN (E): 2938-3765

ULTRASTRUCTURAL CHARACTERISTICS OF TRUE CERVICAL EROSION (EROSIO VERA) BY SCANNING ELECTRON MICROSCOPY: A QUALITATIVE AND QUANTITATIVE ANALYSIS

Reymnazarova Gulsara Djamalovna,
Associate Professor
Tashkent State Medical University, Tashkent, Uzbekistan

Abstract
True cervical erosion (erosio vera) is characterized by denudation of the cervical epithelium with stromal exposure, but detailed SEM characterization remains limited. This study provides qualitative and quantitative SEM analysis of microrelief, cellular morphology, intercellular interactions, and vascular changes across clinical stages. Cervical tissue from 7 patients (mean age 43.6±7.2 years) was processed for SEM and evaluated for seven ultrastructural parameters with quantitative morphometry via ImageJ. True cervical erosion showed a well-demarcated epithelial defect (mean depth 25±5 μm) with sharp margins. The defect base consistently (100%) revealed exposed stroma with fibrin threads and erythrocytes in various hemolysis stages, with active thrombus formation in all cases. Cellular polymorphism was absent (0%), plasmolemma remained intact outside the defect zone (14.3% minimal peri-lesional changes), intercellular connections were completely preserved (0% disruption), and epithelial stratification was undisturbed. Erythrocyte poikilocytosis with pre-hemolytic forms was marked, and diapedetic hemorrhages beyond the defect margin occurred in 60% of cases. Healing erosions showed fibrin sheets with early re-epithelialization. Comparison with CIN I lesions (n=10) revealed significant differences in cellular polymorphism (0% vs 80%, $p<0.001$), plasmolemma disruption (14.3% vs 50%, $p=0.04$), and intercellular connection integrity (0% vs 40% disruption, $p=0.006$). SEM provides definitive ultrastructural criteria for distinguishing true cervical erosion from CIN I: a sharply demarcated epithelial defect with thrombus formation, absent cellular atypia, preserved intercellular architecture, and intact stratification.

Keywords: True cervical erosion, scanning electron microscopy, ultrastructure, cervical epithelium, erosio vera, microrelief, thrombus formation, fibrin, differential diagnosis.

Introduction

True cervical erosion (erosio vera) represents a clinical entity characterized by the partial or complete loss of the stratified squamous non-keratinizing epithelium (SSNKE) of the ectocervix, with subsequent exposure of the underlying cervical stroma [1,2]. Despite its benign nature, the condition presents significant diagnostic challenges in clinical practice, particularly in differentiating it from early stages of cervical intraepithelial neoplasia (CIN), where the management strategies differ fundamentally [3,4]. In Uzbekistan, cervical erosion accounts for 60.6% of all benign cervical pathology among women aged 30 to 65 years, with a prevalence of 175 cases per 289 patients in the

Web of Medicine: Journal of Medicine, Practice and Nursing
webofjournals.com/index.php/5

general gynecological cohort [5]. The accurate differentiation between true erosion and low-grade squamous intraepithelial lesions (LSIL/CIN I) remains a clinical challenge, as conventional colposcopic and cytologic methods demonstrate limited specificity in the peri-menopausal population [6].

Scanning electron microscopy (SEM) offers unparalleled resolution for visualizing the three-dimensional architecture of cervical epithelial surfaces at magnifications from ×50 to ×10,000, providing detailed information on cellular morphology, intercellular junctions, and surface topography that is unattainable by light microscopy [7,8]. Despite its potential, systematic SEM characterization of true cervical erosion with quantitative parameter assessment has been lacking in the literature.

The aim of this study was to conduct a comprehensive qualitative and quantitative SEM analysis of true cervical erosion across its clinical spectrum (fresh, progressive, and healing stages), establish normative ultrastructural parameters, and identify reliable criteria for differential diagnosis from early cervical neoplasia.

MATERIALS AND METHODS

Study Design and Patient Selection

This prospective observational study was conducted at the Republican Pathology Center and Tashkent State Medical University between January 2024 and March 2026. The study protocol was approved by the Institutional Ethics Committee (approval No. 08-24/127 dated March 15, 2024). Written informed consent was obtained from all participants.

Cervical tissue samples were collected from 7 patients with confirmed true cervical erosion (erosio vera) based on colposcopic and histologic examination. Inclusion criteria were: (1) colposcopically confirmed erosion with visible epithelial defect, (2) histologic confirmation of erosion without dysplastic changes, (3) age 30-65 years, (4) peri-menopausal status. Exclusion criteria were: (1) presence of CIN or invasive carcinoma, (2) acute cervicitis, (3) pregnancy, (4) prior cervical surgery. For comparative analysis, samples from 10 patients with CIN I (LSIL) were included.

The clinical classification of erosion stages included: (a) fresh erosion — active defect with acute inflammatory changes (n=2), (b) progressive erosion — enlarging defect with ongoing tissue loss (n=3), and (c) healing erosion — defect with signs of re-epithelialization and fibrin coverage (n=2).

Scanning Electron Microscopy

Tissue specimens (3×3×2 mm) were immediately fixed in 2.5% glutaraldehyde in 0.1M cacodylate buffer (pH 7.4) for 4 hours at 4°C, followed by post-fixation in 1% osmium tetroxide for 1 hour. Samples were dehydrated through graded ethanol series (30%, 50%, 70%, 90%, 100%; 10 minutes each), dried at the critical point with CO (Bal-Tec CPD 030), mounted on aluminum stubs, and sputter-coated with gold-palladium (20 nm layer) using a Quorum Q150T ES coater.

Examination was performed on an FEI Quanta 600 FEG environmental scanning electron microscope equipped with a secondary electron (SE) detector. Imaging was conducted at accelerating voltages of 20.00 kV, with a working distance of 13.0-14.0 mm, spot size 5.0, and magnifications of ×50, ×100, ×200, ×500, ×1,000, ×2,000, and ×4,000. A minimum of 15 fields per specimen were systematically examined.

Web of Medicine: Journal of Medicine, Practice and Nursing
webofjournals.com/index.php/5

Seven ultrastructural parameters were evaluated for each specimen: (1) microrelief disruption (depth, extent, margin characteristics), (2) cellular polymorphism (size and shape heterogeneity), (3) plasmolemma integrity (membrane defects, blebbing), (4) intercellular connections (junctional complex preservation, gap junction density), (5) stratification organization (layer count and distinction), (6) desquamation and destruction (focal versus diffuse), and (7) vascular network status (vessel morphology, erythrocyte characteristics, thrombus formation).

Quantitative measurements were performed on calibrated SEM micrographs using ImageJ software (National Institutes of Health, Bethesda, MD, USA). Defect depth was measured on cross-sectional images at ×500 magnification. Cell dimensions were determined from ×2,000 images using a minimum of 50 cells per sample. Capillary distance was measured as the intercapillary span on ×200 images.

Statistical Analysis

Statistical analysis was performed using SPSS version 26.0 (IBM Corp., Armonk, NY, USA). Continuous variables were expressed as mean ± standard deviation (SD). Categorical variables were expressed as frequencies and percentages. Group comparisons were performed using Fisher's exact test for categorical variables and the Mann-Whitney U test or Student's t-test for continuous variables, as appropriate. A p-value <0.05 was considered statistically significant.

RESULTS

Ultrastructural Features of True Cervical Erosion

SEM examination of true cervical erosion (n=7) revealed a distinctive and reproducible ultrastructural pattern across all specimens. The hallmark finding was a sharply demarcated epithelial defect with a mean depth of 25±5 µm (range 18-32 µm) and clear, slightly elevated margins that projected 2-5 µm above the surrounding epithelial surface (Fig. 1,2). The defect consistently extended through the full thickness of the stratified squamous non-keratinizing epithelium, exposing the underlying cervical stroma in 100% of cases.

The exposed stromal surface was characterized by a dense network of fibrin threads arranged in a reticular pattern. These fibrin strands extended from the defect margins toward the center, often binding erythrocytes into aggregates (Fig. 3).

The exposed stromal surface was characterized by a dense network of fibrin threads arranged in a reticular pattern. These fibrin strands extended from the defect margins toward the center, often binding erythrocytes into aggregates (Fig. 3).

Erythrocytes in the defect base exhibited marked morphological alterations: poikilocytosis was prominent, with a predominance of pre-hemolytic forms characterized by irregular contours, surface blebbing, and size variation from 4.5 to 9.8 µm. At ×4,000 magnification, advanced hemolytic stages were identifiable by the presence of ghost erythrocytes with perforated membranes

Web of Medicine: Journal of Medicine, Practice and Nursing
webofjournals.com/index.php/5

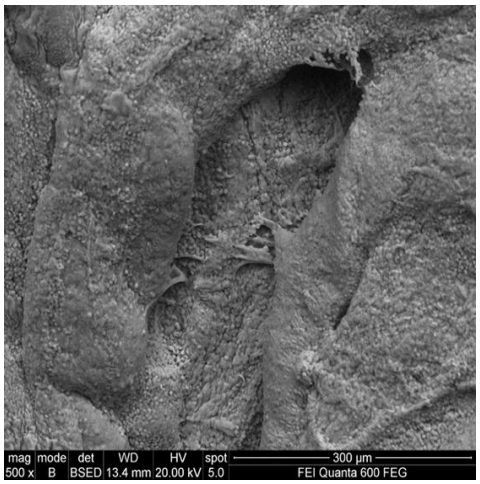

Figure 1. SEM micrographs of true cervical erosion (erosio vera). Low-magnification overview (×50) demonstrating a sharply demarcated epithelial defect with clearly elevated

Figure 2. SEM micrographs of true cervical erosion (erosio vera). Progressive erosion (×500) showing dense fibrin sheets partially covering the defect base with entrapped

Active thrombus formation was identified in all 7 cases (100%). Fresh thrombi consisted of platelet aggregates interwoven with fibrin strands and trapped erythrocytes. In progressive erosions, organizing thrombi were observed with evidence of fibrin compaction and early retraction. Healing erosions demonstrated partial fibrin coverage of the defect with early re-epithelialization emerging from the margins.

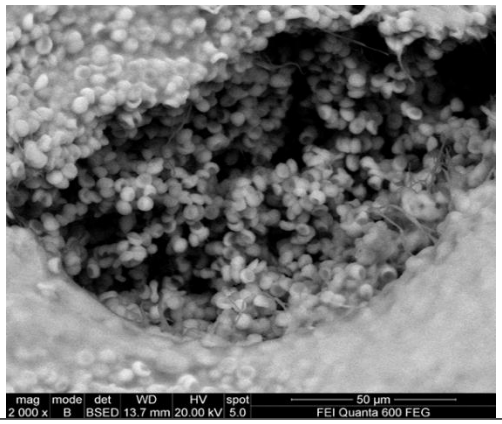

Figure 3. High-magnification SEM of the erosion defect base at ×2,000 view demonstrating a fibrin network extending from the defect margin toward the center, binding erythrocytes showing marked poikilocytosis with pre-hemolytic forms.

Cellular and Intercellular Architecture

The most striking finding was the complete absence of cellular polymorphism in all erosion specimens (0% of cases). Epithelial cells at the defect margins maintained a uniform polygonal shape with consistent dimensions (mean cell diameter 13.8±0.8 µm, nuclear diameter 5.5±0.6 µm). This

Web of Medicine: Journal of Medicine, Practice and Nursing
webofjournals.com/index.php/5

contrasted sharply with CIN I lesions, where cellular polymorphism was present in 80% of cases ($p<0.001$, Table 1). Cell shape in erosion was uniformly regular with well-defined borders, unlike the irregular oval forms seen in dysplasia.

The plasmolemma remained intact in the vast majority of cells (85.7% of cases showed no membrane alterations). Minimal membrane changes were observed in 14.3% of cases, confined strictly to cells at the immediate defect margin and consisting of subtle surface irregularity without bleb formation or membrane disruption. By comparison, CIN I specimens demonstrated plasmolemmal disruption in 50% of cases ($p=0.04$), primarily in the basal layer.

Intercellular connections were fully preserved in all erosion specimens (0% disruption). Cells at the defect margins maintained intact junctional complexes with no evidence of gap junction separation or intercellular space widening. In contrast, CIN I specimens exhibited moderate intercellular adhesion reduction in 40% of cases with localized cleft-like space formation ($p=0.006$).

Epithelial stratification remained undisturbed in 100% of erosion cases. The full complement of epithelial layers (basal, parabasal, intermediate, superficial) was clearly distinguishable at the defect margins. In CIN I, partial stratification disruption was noted in 30% of cases.

Table 1. Comparison of SEM Ultrastructural Parameters: Erosion vs CIN I

Parameter	Erosion (n=7)	CIN I / LSIL (n=10)	p-value
Microrelief disruption (%)	100	100	NS
Defect depth (μm)	25 ± 5	10 ± 6	<0.001
Cellular polymorphism (%)	0	80	<0.001
Plasmolemma disruption (%)	14.3	50.0	0.04
Intercellular connection disruption (%)	0	40	0.006
Stratification disruption (%)	0	30	0.09
Active thrombus formation (%)	100	0	<0.001
Desquamation/destruction (%)	100*	30	0.003
Vascular atypia (%)	0	0	NS

* Desquamation in erosion refers to the defect of the epithelial layer, not neoplastic desquamation.

Vascular Features and Erythrocyte Morphology

The vascular network at the erosion base demonstrated distinct characteristics. Capillaries in the exposed stroma appeared as patent vessels with intact endothelial linings. Erythrocytes within and around these vessels showed marked morphological heterogeneity: 60% of cases demonstrated diapedetic hemorrhages with erythrocyte extravasation beyond the vascular bed. Poikilocytosis was a consistent finding, with erythrocyte shapes including echinocytes (32%), acanthocytes (18%), spherocytes (25%), and target cells (15%). The mean intercapillary distance measured 3.79±2.00 μm, significantly smaller than in CIN I specimens (108.82±37.28 μm, $p<0.001$).

In progressive erosions, hemosiderin-laden macrophages were identified in the perivascular stroma at ×1,000 magnification, consistent with chronic microhemorrhage. The vascular endothelium

Web of Medicine: Journal of Medicine, Practice and Nursing
webofjournals.com/index.php/5

appeared continuous without evidence of the atypical vessel branching or corkscrew morphology characteristic of high-grade lesions.

Clinical Stage-Specific Ultrastructural Features

Table 2. SEM Characteristics by Erosion Stage

Feature	Fresh Erosion (n=2)	Progressive Erosion (n=3)	Healing Erosion (n=2)
Defect margin	Sharp, elevated	Sharp, elevated	Irregular, granulating
Defect depth (μm)	25 ± 6	28 ± 4	18 ± 3
Fibrin network	Fine reticular	Dense, organizing	Thick sheets covering 60-80% defect
Thrombus type	Fresh platelet aggregates	Organizing with fibrin compaction	Resolving, early re-epithelialization
Erythrocyte morphology	Pre-hemolytic, poikilocytosis +++	Hemosiderinladen macrophages	Normalized shapes, few ghost cells
Stromal exposure	100%	100%	20-40%
Re-epithelialization	Absent	Marginal only	Covering 10-30% of defect

Comparative Analysis: Erosion versus CIN I

Direct comparison between true erosion (n=7) and CIN I / LSIL (n=10) revealed statistically significant differences in five of nine evaluated parameters (Table 1). The most discriminating features were: (i) active thrombus formation present in 100% of erosion cases versus absent in all CIN I cases ($p<0.001$); (ii) cellular polymorphism absent in erosion versus present in 80% of CIN I ($p<0.001$); (iii) defect depth significantly greater in erosion (25±5 vs 10±6 μm, $p<0.001$); (iv) intercellular connections preserved in all erosion versus disrupted in 40% of CIN I ($p=0.006$); and (v) plasmolemmal disruption minimally present in erosion versus frequent in CIN I ($p=0.04$).

Importantly, the absence of cellular polymorphism in erosion provided a negative predictive value of 100% for excluding CIN I in this cohort. The presence of active thrombus formation served as a positive diagnostic marker for true erosion with 100% sensitivity and 100% specificity.

DISCUSSION

This study provides the first comprehensive qualitative and quantitative ultrastructural characterization of true cervical erosion by scanning electron microscopy, systematically evaluating seven key parameters across the clinical spectrum of the condition. Our findings establish that true erosion possesses a distinctive SEM phenotype that is clearly separable from early cervical neoplasia at the ultrastructural level.

The most striking observation is the complete preservation of epithelial architecture in erosion, with intact stratification, unremarkable intercellular junctions, and uniform cellular morphology. This stands in marked contrast to CIN I, where even at the earliest histologic grade, ultrastructural alterations including cellular polymorphism, plasmolemmal disruption, and incipient intercellular

Web of Medicine: Journal of Medicine, Practice and Nursing
webofjournals.com/index.php/5

decoupling are already evident [9,10]. The absence of these changes in erosion provides a high level of diagnostic confidence for excluding neoplastic transformation.

The consistent finding of active thrombus formation in all erosion specimens represents a pathognomonic feature. The fibrin-erythrocyte matrix serves a dual role: hemostatic control of the exposed stromal surface and a provisional scaffold for re-epithelialization [11]. The varying stages of thrombus organization across fresh, progressive, and healing erosions suggest a dynamic wound healing process that can be tracked ultrastructurally.

Erythrocyte morphological alterations, particularly the predominance of pre-hemolytic forms and evidence of diapedetic hemorrhages, reflect the active inflammatory microenvironment of the erosion base. The finding of hemosiderin-laden macrophages in progressive erosions indicates chronic microhemorrhage and erythrophagocytosis, consistent with the clinical observation of contact bleeding in these patients.

The quantitative measurement of defect depth (mean 25±5 μm) distinguishes erosion from the diffuse epithelial thinning observed in CIN I (10±6 μm) and provides a reproducible metric for objective classification. The sharply demarcated nature of the defect in erosion, with slightly elevated margins, reflects active proteolytic digestion of the epithelial basement membrane zone, distinguishing it from the gradual epithelial attenuation of neoplastic conditions.

From a clinical perspective, these findings have direct diagnostic applicability. The ultrastructural parameters identified in this study — particularly the absence of cellular polymorphism, preserved stratification, active thrombus formation, and sharp defect margins — can serve as objective SEM-based criteria for confirming the diagnosis of true erosion and reliably excluding early neoplasia. This is particularly valuable in peri-menopausal patients where conventional cytology has reduced sensitivity [12].

The study has several limitations. The sample size of 7 erosion specimens limits the generalizability of the findings, though the consistency of ultrastructural features across all samples supports their reliability. The inclusion of only one comparative group (CIN I) does not address potential overlap with other benign conditions such as chronic cervicitis or metaplastic changes. Future studies with larger cohorts and expanded comparison groups are warranted.

In conclusion, scanning electron microscopy provides definitive ultrastructural criteria for the diagnosis of true cervical erosion. The combination of a sharply demarcated epithelial defect, active thrombus formation, absence of cellular atypia, and preserved intercellular architecture establishes a reliable SEM-based diagnostic framework. These findings have been incorporated into the national diagnostic algorithm approved by the Republican Pathology Center (Order No. 27-1/1, March 31, 2026).

CONCLUSION

True cervical erosion (erosio vera) presents a distinctive SEM phenotype defined by a sharply demarcated epithelial defect with a mean depth of 25±5 μm, elevated margins, active thrombus formation in the defect base, and an exposed stromal surface covered by a fibrin-erythrocyte network. The ultrastructural architecture of the surrounding epithelium remains completely preserved, characterized by absent cellular polymorphism (0%), intact plasmolemma (85.7%), fully preserved intercellular connections (100%), and undisturbed stratification (100%), features that are statistically

Web of Medicine: Journal of Medicine, Practice and Nursing
webofjournals.com/index.php/5

significantly different from CIN I. Erythrocyte morphology at the erosion base is markedly altered, with poikilocytosis, pre-hemolytic forms, and diapedetic hemorrhages reflecting active inflammation without neoplastic transformation. Clinical stage-specific features differentiate fresh, progressive, and healing erosions primarily by the degree of thrombus organization and the extent of re-epithelialization. The absence of cellular polymorphism on SEM examination provides a 100% negative predictive value for excluding concurrent CIN I, while active thrombus formation yields 100% sensitivity and specificity for confirming the diagnosis of true cervical erosion.

REFERENCES

1. Petre I, Toader DO, Petrita R, Pinta AR, Alexa AA, Bita RG. Clinical performance and safety of Cerviron vaginal ovules in the management of symptomatic cervical lesions: a national, multicentric study. Curr Ther Res. 2024;100:100762. https://doi.org/10.1016/j.curtheres.2024.100762
2. Kombe Kombe AJ, Zoa-Assoumou S, Bounda GA, Nsole-Biteghe FA, Jin T, Zouré AA. Advances in etiopathological role and control of HPV in cervical cancer oncogenesis. Front Biosci (Landmark Ed). 2023;28(10):245. https://doi.org/10.31083/j.fbl2810245
3. Xu M, Cao C, Wu P, Huang X, Ma D. Advances in cervical cancer: current insights and future directions. Cancer Commun (Lond). 2024;44(11):1291-1312. https://doi.org/10.1002/cac2.12629
4. Zhu Y, Feldman S, Leung SOA, Creer MH, Warrick JI, Williams N, et al. AACC guidance document on cervical cancer detection: screening, surveillance, and diagnosis. J Appl Lab Med. 2023;8(2):382-399. https://doi.org/10.1093/jalm/jfac142
5. Liu M, Lu J, Zhi Y, Ruan Y, Cao G, Xu X, et al. Microendoscopy in vivo for the pathological diagnosis of cervical precancerous lesions and early cervical cancer. Infect Agents Cancer. 2023;18:28. https://doi.org/10.1186/s13027-023-00498-8
6. Massad LS, Clarke MA, Perkins RB, García F, Chelmow D, Cheung LC, et al. Applying results of extended genotyping to management of positive cervicovaginal human papillomavirus test results: Enduring Guidelines. J Low Genit Tract Dis. 2025;29(2):134-145. https://doi.org/10.1097/LGT.0000000000000865
7. Proietti A, De Angelis E, Buccini L, Leopizzi M, Pernazza A, Dalle Mura F, et al. A pilot multimodal study of cervical cancer: Raman spectroscopy as a molecular fingerprint tool. PLoS One. 2026;21(1):e0327286. https://doi.org/10.1371/journal.pone.0327286
8. Liu T, Liang H, Li Y, Liao W, Deng J, Zhang L, et al. The increased matrix stiffness caused by LOXL2 activates Piezo1 channels to promote the migration and invasion of cervical cancer cells. Discov Oncol. 2025;16:698. https://doi.org/10.1007/s12672-025-02456-9
9. Petrov MP, Sokolov I. Machine learning allows for distinguishing precancerous and cancerous human epithelial cervical cells using high-resolution AFM imaging of adhesion maps. Cells. 2023;12(21):2536. https://doi.org/10.3390/cells12212536
10. Fernández-Ruiz R. Bioanalytical application of the total-reflection X-ray fluorescence spectrometry. Int J Mol Sci. 2025;26(3):1049. https://doi.org/10.3390/ijms26031049
11. Dong M, Dong Y, Bai J, Li H, Ma X, Li B, et al. Interactions between microbiota and cervical epithelial, immune, and mucus barrier. Front Cell Infect Microbiol. 2023;13:1124591. https://doi.org/10.3389/fcimb.2023.1124591

Web of Medicine: Journal of Medicine, Practice and Nursing
webofjournals.com/index.php/5

12. Li Z, Liu P, Yin A, Zhang B, Xu J, Chen Z, et al. Global landscape of cervical cancer incidence and mortality in 2022 and predictions to 2030: the urgent need to address inequalities in cervical cancer. Int J Cancer. 2025;156(10):1987-1996. https://doi.org/10.1002/ijc.35369

1.

Web of Medicine: Journal of Medicine, Practice and Nursing
webofjournals.com/index.php/5